Journal of Biomolecular NMR, 4 (1994) 367–384
ESCOM

J-Bio NMR 180

Sequence-dependent conformational heterogeneity of a hybrid DNA · RNA dodecamer duplex

Xiaolian Gao[a,b] and Peter W. Jeffs[b]

[a]*Department of Chemistry, University of Houston, Houston, TX 77204-5641, U.S.A.*
[b]*Structural & Biophysical Chemistry, Glaxo Inc., Research Institute, Research Triangle Park, NC 27709, U.S.A.*

Received 3 May 1993
Accepted 5 November 1993

Keywords: 2D NMR; 3D NMR; Hybrid duplex; Oligonucleotide; Conformation; Structure

SUMMARY

Two- and three-dimensional homonuclear NMR studies of a hybrid duplex RI, formed by annealing r(GCGCAAAACGCG) and d(CGCGTTTTGCGC) strands are described. NMR parameters, such as intra- and interresidue proton–proton NOEs and sugar proton coupling constants were analyzed with reference to those of the corresponding DNA · DNA duplex. Furthermore, spectral analyses were conducted on the basis of model structures of nucleic acid duplexes. Distinctive spectral patterns of the hybrid duplex reveal unique heterogeneous conformations which co-exist throughout the sequence and are significantly different from those of model structures of either canonical A- or B-forms. Features of an intermediate conformation were observed in the DNA and RNA strands in duplex RI, the former being more B-like and the latter more A-like. Three-dimensional NOESY-NOESY spectra were analyzed and their use was demonstrated for resolving superimposed resonances and cross peaks, especially those originating from the RNA strand. The application of a useful strategy that combines the use of 2D NMR data and the known structural information for efficient 3D spectral analyses is demonstrated.

INTRODUCTION

Because of the crucial role of DNA · RNA hybrid complexes in transcriptional and replicational processes, investigation of the structural features induced by hybrid duplex formation has been the focus of a wide range of biochemical, chemical and physical studies. Fiber diffraction, circular dichroism and Raman measurements on synthetic polymers (Milman et al., 1967; O'Brien and MacEwen, 1970; Gray and Ratcliff, 1975; Zimmerman and Pheiffer, 1981; Shindo and Matsumoto, 1984; Arnott et al., 1986; Steely et al., 1986; Benevides and Thomas, 1988) have led to the general agreement that sugar puckers in hybrid duplexes occur in two types of conformation,

Supplementary material available from the authors: tables containing torsion angles of A- and B-form nucleic acid complexes and relative NOE intensities of DNA · DNA duplex I and DNA · RNA duplex RI.

which are characterized by a C3'-endo RNA strand and a C2'-endo DNA strand. However, the conclusions with regard to helical characteristics differed; A- (Milman et al., 1967), B- (Gupta et al., 1985) and intermediate forms (Arnott et al., 1986) were proposed for various polymer sequences. Several oligonucleotide and DNA · RNA chimeric hybrid duplexes have been examined by NMR and by single-crystal crystallography. Depending on the sequence, the data suggested the existence of A-, B- and intermediate forms (Wang et al., 1982; Mellema et al., 1983; Reid et al., 1983; Happ et al., 1988; Chou et al., 1989; Katahira et al., 1990; Hall and McLaughlin, 1991; Heus and Pardi, 1991; Egli et al., 1992; Wang et al., 1992; Jaishree et al., 1993). In one example, the crystalline duplex (r(GCG) · d(TATACGC))$_2$ was found in a conformation close to the A-form (both ribose and deoxyribose sugars were in the C3'-endo conformation), but this duplex underwent a conformational transition in solution, with the deoxynucleotide residues adopting a C2'-endo form (Wang et al., 1982; Mellema et al., 1983).

The seemingly inconsistent findings of some of these previous studies may be explained by recognizing that the conformational variation in these hybrid duplexes is not only sequence dependent, but that in certain cases conformational changes may be induced by medium effects. In line with this notion, there is increasing evidence of the importance of structural heterogeneity as a basis for enzyme recognition, as it pertains to deviations from A- or B-form by the substrate hybrid duplexes. For instance, ribonuclease H appears to discriminate irregular structural features of hybrid duplexes, rather than recognizing sequences in the substrate helical region (Nakamura et al., 1991). This in particular demonstrates the need for detailed investigation of structures of a range of hybrid duplexes to improve our understanding of the structure–function relationships of these molecules in biological systems. Another motivation is the recent demonstration of the potential of using synthetic oligodeoxyribonucleotides as antisense agents, which specifically target RNA sequences important for gene regulation. In this area, we need to understand the structural basis of molecular interactions that underlie the specific recognition of RNA sequences. Such information is crucial for developing nucleic acid-binding molecules with improved binding specificity and affinity.

The high-resolution multidimensional NMR techniques developed in the last few years provide an opportunity to obtain detailed solution structural information on hybrid duplex structures. In this report we describe the two- and three-dimensional (2D and 3D) homonuclear NMR study of a nonselfcomplementary dodecamer hybrid duplex d($C_1G_2C_3G_4T_5T_6T_7T_8G_9C_{10}G_{11}C_{12}$) · r($G_{101}C_{102}G_{103}C_{104}A_{105}A_{106}A_{107}A_{108}C_{109}G_{110}C_{111}G_{112}$) (designated duplex RI). The purpose of this study was twofold. First, we wanted to compare the structural requirements for hybridization of a single-stranded DNA with an RNA strand vs. hybridization with a DNA strand; second, we wanted to explore the application of 3D NMR methods, which will be applicable for further studies of hybrid duplexes containing modified nucleotide analogs.

MATERIALS AND METHODS

Syntheses of oligonucleotides

The DNA strand d(CGCGTTTTGCGC) of duplex RI was synthesized as reported (Gao et al., 1992). The RNA strand r(GCGCAAAACGCG) was synthesized on an ABI 380B using phosphoramidite chemistry on a 10-μmol scale. The trityl group was removed after the synthesis and the base-protecting groups were removed by heating in NH_4OH/EtOH (3:1) at 55 °C for

16 h. The 2'-O-*t*-butyldimethylsilyl groups were cleaved with a 24-h treatment at room temperature, using 1 M tetrabutylammonium fluoride (TBAF) at a molar ratio of 3000:1 (TBAF:RNA). The sample volume was reduced to about half and an equal volume of 1 M triethylammonium acetate (TEAA) was added. The product mixture was applied to a C_4 Vydac column (2.2 × 25 cm) and eluted using a 0–40% B gradient over 30 min where A = 0.1 M TEAA and B = CH_3CN. The RNA was desalted using a C_{18} column and eluted at 15 ml/min with H_2O for 20 min; a 0–100% B gradient was then used to elute the RNA off the column, where A = H_2O and B = CH_3CN. The purified RNA was characterized by electrospray mass spectrometry and its purity was determined by ion exchange HPLC (Dionex Nucleopac 4.6 × 25 cm, 0–100% B over 30 min at 1.5 ml/min, where A = 25 mM Tris, pH 8.0 and B = 25 mM Tris, 1 M KCl, pH 8.0).

1D and 2D NMR experiments

All NMR experiments were performed on Bruker AMX 500 and 600 MHz spectrometers. Single-stranded d(CGCGTTTTGCGC) and r(GCGCAAAACGCG), when titrated at room temperature in pH 6.3 aqueous buffer, form duplex RI as monitored by 1D proton spectra. The final NMR samples contained 2–3 mM of the duplex in aqueous buffer (0.1 M NaCl, 5 mM phosphate, 0.1 mM EDTA, pH 6.2). The range of the nonselective spin-lattice relaxation times T_1 of protons was estimated in D_2O solution, using an inversion recovery pulse sequence [repetition delay – 180° (H) – recovery delay – 90° (H) – acq.]. The repetition delay was 15 s and the results showed that except for H2 protons of adenine residues most proton T_1 values were less than 2.17 s (the null point was less than 1.5 s). This result is consistent with that reported by Hoffman et al. (1993) for an NMR study of an RNA structure. 2D proton NMR spectra were collected in H_2O and D_2O. NOESY spectra were obtained at 15 °C in H_2O solution, using mixing times of 100 and 150 ms. Various COSY experiments, including DQF-COSY, TOCSY (with 82 and 152 ms isotropic mixing times), COSY-35 and NOESY experiments (100 and 250 ms mixing times) were obtained in D_2O solution at 30 °C. A separate set of NOESY data was acquired at 22 °C, using 100 and 250 ms mixing times. In all 2D NMR experiments, repetition delays varied between 1.5–2.0 s. NMR data contained 2048 complex data points in the t_2 dimension and 512–1024 real points in the symmetrical t_1 dimension, and were processed and analyzed using the FELIX program (Biosym/Hare Research). Interproton distances were estimated from NOE connectivities on the basis of a two-spin approximation (Neuhaus and Williamson, 1989). Scalar coupling constants for sugar H1'-H2' and H1'-H2" protons were measured from the antiphase multiplets of COSY-35 cross peaks along the F2 dimension; the coupling constants of H3'-H4' protons were estimated from both the magnitude and patterns of the cross peaks of various COSY spectra.

3D NOESY-NOESY experiment

The 3D experiment was conducted in D_2O solution at 30 °C, according to the protocol described previously (Boelens et al., 1989; Gao and Burkhart, 1991). The 3D spectrum covered a spectral width of 8.33 ppm (4166 Hz) in each of the three dimensions and was recorded with 200 ms of NOE mixing times in both steps of magnetization transfer. The data set consisted of 512 × 64 × 100 complex points in the ω_3, ω_2 and ω_1 dimensions, respectively. Data processing was carried out with the FELIX program; a 90° shifted sine-bell function was applied to all three dimensions to give a final matrix containing 512 × 256 × 256 data points. The 3D spectrum was analyzed mainly through the planes of interest, which intersect with the ω_3 axis (ω_3 is a constant).

^{31}P NMR spectroscopy

A ^{31}P 1D spectrum was obtained with ^{1}H decoupling and it was referenced to the resonance of external trimethyl phosphate, dissolved in aqueous buffer (0.1 M NaCl, 10 mM phosphate, pH 6.2). A ^{1}H-detected ^{31}P-^{1}H correlation spectrum was recorded according to a reported pulse sequence (Sklenář et al., 1986), with the ^{31}P 90° pulse cycling in phase with the receiver. Spectral widths were 500 and 1562 Hz for the ^{31}P and ^{1}H dimensions, respectively.

Model structures

Reference distances used for NOE analysis were calculated from the standard A- and B-form models, which were based on the fiber diffraction structural parameters of Arnott and Hukins (1972,1973) and were provided by the INSIGHT program (Biosym). A list of torsion angle parameters for the A- and B-form nucleic acid duplexes and a list of pertinent references are available from the supplementary material (Table S1).

RESULTS AND DISCUSSION

This study emphasizes comparison of the DNA · RNA hybrid duplex RI with its well-characterized DNA · DNA counterpart d(CGCGTTTTGCGC) · d(GCGCAAAACGCG) (designated duplex I; Gao et al., 1992). Using such a systematic comparative approach, uncertainties associated with the derivation of the structural parameters can be reduced and important structural information revealed. Furthermore, in this study structural correlation of the experimental results will be illustrated by their comparison with model A- or B-form duplexes. In addition, to address spectral overlaps of natural RNA sequences, we discuss the advantages and the limitations of the use of the homonuclear 3D NOESY-NOESY experiment for the analysis of the hybrid duplex RI.

Proton chemical shifts and correlation to helical conformation

The majority of proton resonances were assigned based on the observed through-bond and through-space connectivities, typical of a right-handed helical sequence (Wüthrich, 1986). Their values are given in Table 1, along with chemical shift differences between the hybrid duplex RI and the corresponding DNA · DNA duplex I. Generally, nonexchangeable base protons, H1', H2' and H2" exhibited narrower chemical shift dispersion in the hybrid duplex RI. For instance, base protons (terminal ones were excluded) of the DNA and RNA strands in duplex RI resonated between 7.26–7.89 and 7.33–7.88 ppm, as compared to 7.11–7.81 and 6.93–8.02 ppm observed for their counterparts in duplex I. A similar comparison of H1' proton resonances in the DNA and RNA strands in duplex RI showed chemical shift ranges of 5.80–6.08 and 5.20–5.78 ppm, whereas the corresponding parameters in duplex I are 5.55–6.04 and 5.27–5.89 ppm, respectively. The reduction in chemical shift dispersion in duplex RI is mainly due to downfield shifted pyrimidine resonances and, conversely, upfield shifted purine resonances (Table 1). As a consequence of the reduction in chemical shift dispersion, resonance and cross-peak assignments became more difficult for the hybrid duplex RI. In an NMR study of a dodecamer hybrid duplex, Chou et al. (1989) reported a similar pattern, in which the chemical shifts of the base protons of the DNA strand became less dispersed in a hybrid duplex. These results suggest that the narrower distribution of base and H1' proton chemical shifts is characteristic of hybrid duplexes.

Significant changes in proton chemical shifts were detected for the DNA strand in the

TABLE 1
CHEMICAL SHIFTS OF HYBRID DNA · RNA DUPLEX RI[a] AND CHEMICAL SHIFT DIFFERENCES BETWEEN DUPLEXES RI AND I[b]

	HN	NH_2	H8	H2	H6	H5	H1'	H2'	H2"	H3'	H4'
dC1					7.69	5.89	5.89	2.07	2.46	4.65	4.05
dG2	12.95		7.89				5.96	2.63	2.72	4.89	4.34
dC3		8.32/6.44			7.37	5.27	5.95	2.39	2.51	4.73	4.24
dG4	12.71		7.45				5.94	2.49	2.68	4.69	4.28
dT5	14.09				7.32	1.14	6.04	2.20	2.60	4.77	4.25
dT6	13.75				7.46	1.51	6.08	2.21	2.62	4.83	4.20
dT7	13.69				7.44	1.55	6.05	2.15	2.60	4.81	4.19
dT8	13.11				7.36	1.59	5.96	2.28	2.54	4.87	4.17
dG9	12.05		7.55				5.80	2.43	2.55	4.85	4.29
dC10		8.14/6.19			7.26	5.06	5.81	2.20	2.43	4.69	4.16
dG11	12.71		7.56				5.91	2.43	2.62	4.78	4.26
dC12		8.14/6.50			7.31	5.11	6.11	2.02	2.17	4.41	4.01
rG101	12.72		7.85				5.52	4.63		4.43	4.20
rC102		8.28/6.41			7.64	5.15	5.46	4.52		4.44	4.36
rG103	12.82		7.53				5.60	4.44		4.51	4.38
rC104		8.12/6.67			7.51	5.18	5.26	4.45		4.37	4.33
rA105			7.88	6.62			5.68	4.47		4.40	
rA106			7.78	7.08			5.67	4.41		(4.58)	(4.54)
rA107			7.76	7.14			5.66	4.40		4.52	
rA108			7.83	7.66			5.78	4.40		4.45	4.39
rC109		8.06/6.69			7.33	5.12	5.20	4.26		4.30	4.40
rG110	12.85		7.51				5.58	4.29		4.51	
rC111		8.34/6.71			7.49	5.17	5.44	4.08		4.40	4.25
rG112			7.72				5.79	4.11		4.29	4.17
Shift differences between duplexes RI and I											
dC1					0.24	0.18	0.30	0.28	0.21	0.10	0.11
dG2	0.01		0.08				0.19	0.09	0.10	0.04	0.11
dC3					0.17	0.02	0.40	0.48	0.22	0.01	0.17
dG4	−0.11		−0.34				0.03	−0.04	−0.05	−0.17	−0.01
dT5	0.08				0.21	−0.17	0.14	0.20	0.11	0.04	0.10
dT6	−0.15				0.13	0.03	0.04	0.11	0.10	0.05	0.12
dT7	−0.06				0.11	0.02	0.05	0.11	0.08	0.02	0.10
dT8	−0.48				0.20	0.03	0.27	0.35	0.21	0.09	0.16
dG9	−0.49		−0.20				0.12	−0.10	0.02	−0.01	0.04
dC10					0.08	−0.16	0.25	0.40	0.22	0.01	0.13
dG11	−0.28		−0.15				0.12	−0.01	0.04	−0.05	0.06
dC12					0.15	0.07	0.13	−0.06	0.09	0.06	0.13

[a] Values for exchangeable protons were from a 150-ms mixing time NOESY, recorded in 0.1 M NaCl, 10 mM PO_4, and 0.1 mM EDTA, 290 K, pH 6.2 with chemical shifts referenced to the HOD resonance at 4.80 ppm; values for non-exchangeable protons were from a 250-ms mixing time NOESY, recorded at 303 K with chemical shifts referenced to the HOD resonance at 4.65 ppm. Ambiguities are indicated by parentheses.

[b] Chemical shifts of duplex I were reported previously (Gao et al., 1992). $\Delta\delta = \delta$(duplex RI) − δ(duplex I). A negative value indicates an upfield shift.

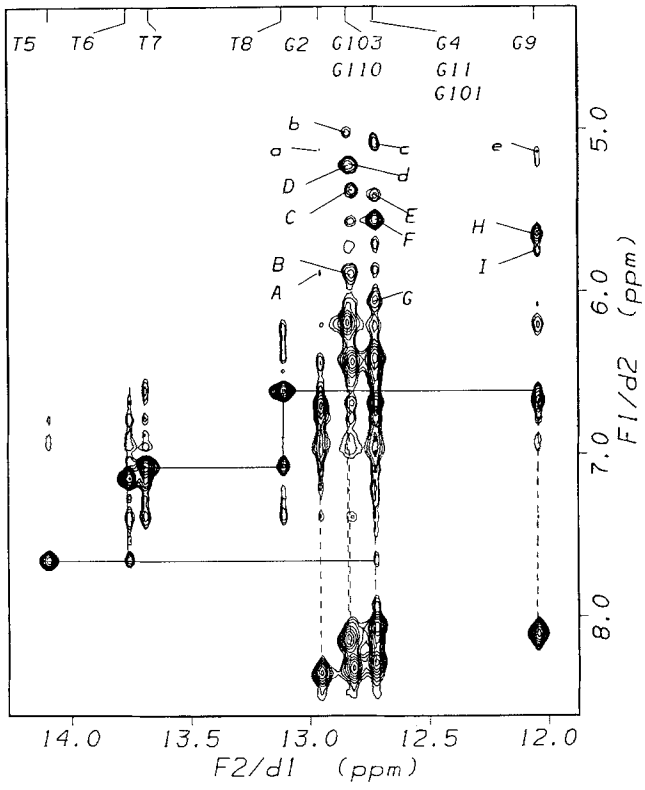

Fig. 1. Expanded 2D NOESY (150 ms mixing time) spectrum of duplex RI, recorded in H_2O as described in the Materials and Methods section. The spectral region covers imino resonances in F2 and base and H1' resonances in F1, respectively. Assignments of imino protons are given at the top of the spectrum. Connectivities from adenine H2 to adjacent protons are traced by solid lines and those from guanine imino protons to cytidine amino protons are shown by dashed lines. NOEs linking guanine imino with cytidine H5 protons are shown by lower case symbols; those linking guanine imino with H1' protons are shown by capital lettering. a: G2(HN)/C111(H5); b: G103(HN)/C10(H5); c: G4(HN)/C109(H5) and G11(HN)/C102(H5); d: G110(HN)/C3(H5); e: G9(HN)/C104(H5); A: G2(HN)/C3(H1'); B: G103(HN)/G11(H1') and G110(HN)/G4(H1'); C: G110(HN)/C111(H1'); D: G103(HN)/C104(H1'); E: G101(HN)/C102(H1'); F: G4(HN)/G110(H1') and G11(HN)/G103(H1'); G: G4(HN)/T5(H1'); H: G9(HN)/A105(H1'); I: G9(HN)/G9(H1').

DNA · RNA duplex RI as compared to that in the DNA · DNA duplex I (Table 1). This clearly reflects a conformational change in the DNA strand as a consequence of the binding to the RNA strand. This result indicates that a DNA sequence may assume distinctively different structures, conferred by its complementary partner strand.

Spectral analysis of the central A4 · T4 segment

We will discuss spectral patterns associated with adenine H2 of the central A4 · T4 residues in this section. A(H2) protons are located in the minor groove and make contacts with a number of adjacent protons of both the same strand and the opposite strand. The interactions between A(H2) and Watson–Crick imino protons are presented in the expanded NOESY spectrum, in the regions 11.8–14.2 ppm (F2) and 4.2–8.5 ppm (F1) (Fig. 1). In this figure, sequential connectivities of thymine HN_i to adenine $H2_j$ as well as HN_{i+1} to $H2_j$ can be followed by solid lines, linking the

central six-residue G4–G9 segment. Two interesting features can be recognized. First, A105(H2) and T8(HN) protons of the same hybrid base pair in duplex RI exhibit the largest shifts (> 0.4 ppm upfield) relative to those of the DNA · DNA base pair in duplex I. This is indicative of a major structural difference, the details of which are under investigation. Second, in comparison to DNA · DNA duplex I, relative NOE intensities of sequential H2/HN vs. intra-base-pair H2/HN connectivities become weaker in duplex RI (Table 2). This reduction in NOE intensities can be attributed to an A-type structure, which is characterized by somewhat larger separations between sequential H2 and HN protons (Table 2).

Adenine H2 protons are also in close vicinity to a number of nonexchangeable protons, that are better detected in NOESY spectra recorded in D_2O (Table S2, supplementary material). An example covering the spectral regions of F1 5.0–6.2 ppm and F2 6.6–8.0 ppm is shown in Fig. 2. In this spectrum, NOEs linking A(H2) with H1' of residue i+1 are moderate and those of the cross-strand adenine $H2_i/H1'_{j+1}$ are more intense. This spectral pattern is in contrast to that of DNA · DNA duplex I, where all H2/H1' NOEs, whether sequential or interstrand, are of comparable intensity. A segment of consecutive adenine residues in oligonucleotides often exhibits a trend where the intensities of H2/H1' NOE cross peaks progressively increase from the 5'- to the 3'-direction, due to narrowing of the minor groove (Katahira et al., 1990; Chen et al., 1992). Such a spectral pattern was not observed in duplex RI, suggesting the unique structural feature associated with the DNA A4-track is not present in RNA sequences. Despite these spectral differences, we detected sequential NOEs between adjacent adenine H2 protons, similar to what was observed in DNA · DNA duplex I.

Collectively, the observed differences in NOE patterns between the hybrid duplex RI and the DNA · DNA duplex I are not a simple reflection of the differences predictable from comparing an A-form with a B-form duplex. For example, the adenine H2/H2 separation between adjacent residues increases from 3.8 Å (B-form) to 4.9 Å (A-form), but similar NOE intensities were observed in both duplexes RI and I. If duplex RI adopted a typical unperturbed A-form, a

TABLE 2
IMINO (HN) AND ADENINE H2 NOE COMPARISON OF DNA · DNA DUPLEX I AND DNA · RNA DUPLEX RI[a]

Proton pair		NOE		Model distance	
		DNA · DNA	DNA · RNA	B-form	A-form
A108(H2)	T5(HN)	m	m	2.92	2.93
A108(H2)	T6(HN)	m−	w	3.92	4.47
A108(H2)	G4(HN)	w	v.w	3.79	4.45
[b]					
A105(H2)	T8(HN)	m+	m	2.92	2.93
A105(H2)	G9(HN)	w+	w−	4.30	4.99
A105(H2)	T7(HN)	v.w	w−	5.22	5.82

[a] The experimental conditions were given in the legend to Table 1. The majority of the NOE intensities are from a 100-ms NOESY. Symbols for NOE intensities: s, strong; m, medium; w, weak; −/+, weaker or stronger than the indicated intensity.

[b] The central A106 and A107-related NOE patterns are similar in both sequences.

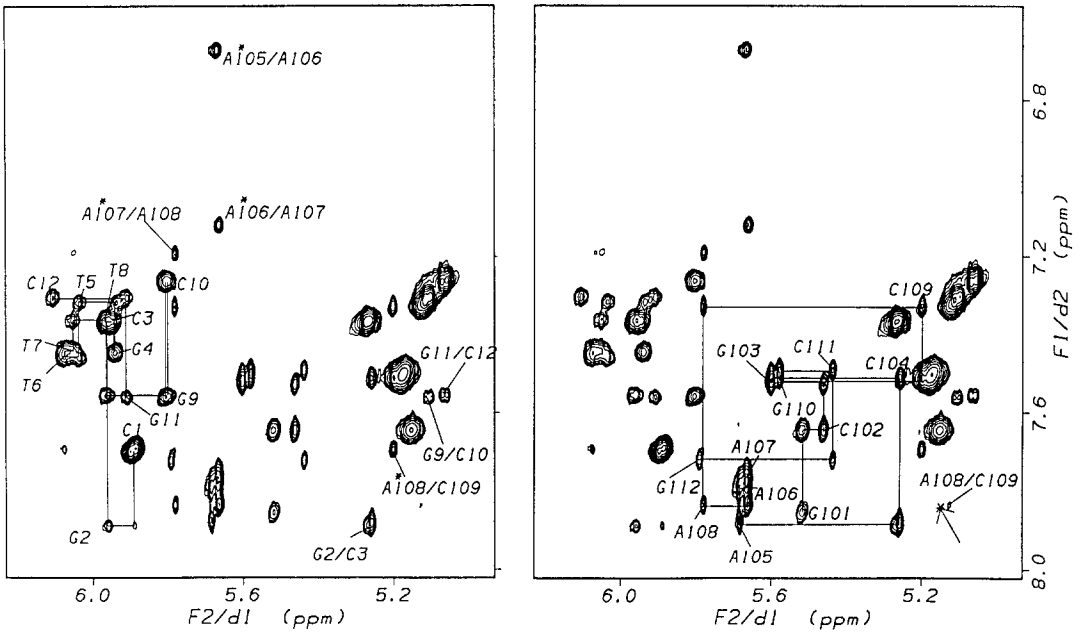

Fig. 2. Expanded 2D NOESY (250 ms mixing time) spectrum of duplex RI, recorded in D_2O as described in the Materials and Methods section. The spectral region covers H1' resonances in F2 and base protons in F1, respectively. The plot on the left displays base/H1' connectivities (cross peaks linked by solid lines) of the DNA strand. Proton–proton contacts between adenine H2 and adjacent H1' (A105/A106, A106/A107, A107/A108, A108/C109) and between purine H8 and adjacent cytidine H5 (G2/C3, G9/C10, G11/C12) are also indicated. The plot on the right displays base/H1' connectivities (cross peaks linked by solid lines) of the RNA strand. Proton–proton contacts between purine H8 and adjacent cytidine H5 residues for A108/C109 are also indicated; such connectivities were either overlapped or absent for other residues.

sequential adenine H2/H2 NOE would not have been observed. This discrepancy between observed NOEs and model distances suggests that a base-stacking variation from typical A-form exists in duplex RI.

Spectral analysis related to base–base interactions

Watson–Crick imino proton connectivities in duplex RI were examined by using NOESY data sets obtained at different mixing times; the results are summarized in Table 3. With the exception of the proton contacts at the T8-G9 step, the NOE cross peaks from hybrid duplex RI paralleled those from duplex I (Table 3). In the spectra of duplex I there was an NOE of moderate intensity between the T8-G9 imino protons, whereas no such an NOE was observed in the spectra of the hybrid duplex RI. Judging from model distances listed in Table 3, the absence of the NOE in the DNA strand of duplex RI can be correlated to the increased proton–proton separation at the T-G step (Table 3) in A-type base stacking. On the other hand, many distance violations of the A-form were detected in duplex RI, indicating marked structural deviations from the canonical A-form. For instance, imino-imino proton separation between adjacent thymine residues in an A-form duplex is 3.9 Å, which should give rise to a very weak NOE, but experimentally, moderate NOEs were detected in both duplexes RI and I (Table 3).

An interesting difference was observed in NOEs connecting sequential base protons (Table S2, supplementary material). Although base proton–proton separations in pyrimidine–pyrimidine, purine–purine, purine–pyrimidine and pyrimidine–purine dimeric units are similar in B- or A-type structures, it was only in the DNA strands of hybrid duplex RI that we observed such sequential base–base proton NOEs. Although it appears reasonable to attribute such NOEs to helical conformational heterogeneity, we note that this experimental result cannot be directly correlated to model structures, but can be rationalized as follows. The base–base proton (H8 and H6) NOEs originate from an indirect interaction, which is mediated by H1' protons ($H8_i$, $H6_i/H1'_{i,i-1}/H8_{i-1},H6_{i-1}$) due to spin diffusion. Indeed, base–base proton NOEs were not observed when 100-ms NOESY spectra were recorded for duplexes RI and I. Thus, the presence of base–base proton NOEs in the DNA strand of duplex RI suggests closer contacts between base H8,H6 and H1' protons, whereas the absence of these NOEs in the RNA strand reflects a larger separation of base H8,H6 and H1' protons. These results are consistent with a B-type DNA strand and an A-type RNA strand in duplex RI.

Various proton monitors of base–base interactions described above, including HN–HN and base–base protons, exhibited a spectral pattern characteristic of mixed A- and B-duplex in the hybrid duplex RI. Although a detailed structure description must rely on the final computational modeling studies, the implication is that in duplex RI, the stacking or the relative orientation of the bases is not in any standard form and their conformations in the two strands are different.

Sequential base–sugar NOE connectivities

Intra- and interresidue NOEs related to nonexchangeable base and sugar protons of duplex RI

TABLE 3
SEQUENTIAL IMINO–IMINO PROTON CONNECTIVITY COMPARISON OF DNA · DNA DUPLEX I AND DNA · RNA DUPLEX RI[a,b]

DNA · DNA		NOE	DNA · RNA		NOE	Adjacent bases
G112(HN)	G2(HN)	absent	rG112(HN)	dG2(HN)	absent	CG
G110(HN)	G2(HN)	m−	rG110(HN)	dG2(HN)	absent	GC
G110(HN)	G4(HN)	[c]	rG110(HN)	dG4(HN)	ov, m	CG
T5(HN)	G4(HN)	m+	dT5(HN)	dG4(HN)	m	GT
T5(HN)	T6(HN)	m	dT5(HN)	dT6(HN)	m	TT
T7(HN)	T6(HN)	m	dT7(HN)	dT6(HN)	m	TT
T7(HN)	T8(HN)	m	dT7(HN)	dT8(HN)	m	TT
G9(HN)	T8(HN)	m	dG9(HN)	dT8(HN)	absent	TG
G9(HN)	G103(HN)	w	dG9(HN)	rG103(HN)	w	GC
G11(HN)	G103(HN)	absent	dG11(HN)	rG103(HN)	ov	CG
G11(HN)	G101(HN)	absent	dG11(HN)	rG101(HN)	absent	GC

[a] The experimental conditions were given in the legend to Table 1. The majority of the NOE intensities are from a 100-ms NOESY. Symbols for NOE intensities: s, strong; m, medium; w, weak; −/+, weaker or stronger than the indicated intensity.

[b] For B-form, distances (Å) of dimeric segments are CG = 3.73, GC = 3.28, GT = 3.49, TT = 3.49, TG = 4.13; and for A-form, distances (Å) are CG = 4.57, GC = 3.46, GT = 3.40, TT = 3.90, TG = 5.01.

[c] Cross peak too close to the diagonal.

were assigned by analyzing 2D and 3D spectra. Examples of base proton/H1' connectivities are shown in Fig. 2. The identification of the similarities and differences between duplexes RI and I and the comparison of their features with model A- and B-structures are summarized below (Table S2, supplementary material): (a) For the DNA strand in duplex RI the H8,H6/H1' NOEs are moderate to weak and most sequential base proton/H1' NOEs are slightly stronger than intraresidue NOEs. The NOE patterns of the DNA strand in duplex RI are comparable to those observed in duplex I, although their intensities are slightly reduced. These observed NOEs resemble those expected for a B-type structure, which is characterized by a shorter interresidue base proton/H1' separation (2.8 Å) compared to the intraresidue base proton/H1' distance (3.7–3.9 Å). Conversely, the overall features of the NOE patterns of the RNA strand closely resemble an A-type structure with shorter intraresidue base proton/H1' separations compared to those of the corresponding base proton/H1' interresidue distances (Table S2, supplementary material). (b) Pyrimidine H5 protons in the DNA strand of duplex RI exhibit weak NOEs to sequential H1' protons, while no observable NOE intensity was found from the H5/H1' cross peaks in the RNA strand (Table S2, supplementary material). In the A-form model, the H5/H1' separation is greater than 4.9 Å, compared to the 3.7 Å interresidue H5/H1' distance in a B-form helix. (c) Predicted patterns of relative NOE intensities for H8,H6/H2'(intra), H8,H6/H2"(intra), H8,H6/H2'(inter) and H8,H6/H2"(inter) for B- and A-form duplexes are characteristically different. In a B-form duplex the H8,H6/H2'(intra) NOE is relatively stronger than the H8,H6/H2"(intra) NOE, whereas the opposite is true in an A-form duplex. Conversely, the H8,H6/H2'(inter) NOE is relatively weaker than the H8,H6/H2"(inter) NOE in a B-form duplex, but stronger in an A-form duplex. Experimentally, the DNA strand in duplex RI exhibited B-like sequential NOE patterns with NOE(base proton/H2') weaker than NOE(base proton/H2") and the RNA strands exhibited strong interresidue base proton/H2' NOEs, characteristic of an A-like helix. Moreover, it was observed that the intensities of the sequential NOEs were reduced at the A105–A107 region in duplex RI (Table S2, supplementary material). (d) In models of A- and B-form duplexes, base H5 protons should be in close proximity to sequential H2' protons (3.0 and 3.2 Å, respectively) and even closer to H2" protons in B-form helices (2.8 Å). NMR data showed that both DNA and RNA strands exhibited only weak to moderate NOEs for sequential H5/H2' connectivities, indicating deviation of the helical geometry from classical A- or B-forms. (e) Both DNA and RNA strands in RI exhibited weak to moderate NOEs connecting H8,H6 base protons with H3' of the same residue and of sequential residues, even though strong intraresidue H8,H6/H3' NOEs are anticipated for the typical A-form (Table S2, supplementary material). In this category, the general pattern of the NOEs of duplex RI reflects closer intraresidue than interresidue contacts and their intensities are comparable to those derived from duplex I. These results are suggestive of B-like structural characteristics for both strands in RI. (f) With respect to H5/H3' NOEs, the only observed cross peak was a weak NOE between H5 of C10 and H3' of G9 of duplex RI. It is important to note that for an A-form duplex the interresidue H5/H3' distance is 3.6 Å, which is expected to lead to an observable NOE of medium intensity.

In summary, although qualitative, a detailed analysis and comparison of NOEs correlating base H8,H6 to sugar H1', H2', H2" and H3' protons clearly demonstrate a heterogeneous conformation of duplex RI, featuring a combination of A-, B- and intermediate type of structural characteristics. It is evident that conformational differences are distributed along the sequence as well as between the DNA and RNA strands, with the former more B-like and the latter more

A-like. Quantitative treatment of these results should provide a solution structural model for the hybrid DNA · RNA duplex RI.

COSY spectra and sugar pucker

Sugar proton coupling constants were measured with an accuracy of ±0.5 Hz from the COSY-35 spectrum, in which passive couplings are partially cancelled. Such measurements for duplex RI generated coupling constants for H1'/H2' (DNA and RNA strands), H1'/H2" (DNA strand) and apparent coupling constants for H3'/H4' (DNA strand) (Table 4). $J_{3',4'}$ couplings in the DNA strand were obtained with H2',H2" decoupling and were unobtainable in the RNA strand due to the near coincidence of the ribose H3' and H4' resonances. The observed coupling constants reflect some characteristic trends and important features. With the exception of the two 3'-terminal residues, sugars in the RNA strand exhibit small H1'/H2' coupling constants (< 2 Hz), indicating that the ribose sugars of the hybrid duplex RI prefer a C3'-endo conformation (sugar dihedral angle C5'-C4'-C3'-O3'(δ) ~ 80°). $J_{1',2'}$ couplings of the DNA strand in duplex RI are of reduced magnitude, compared to their counterparts in duplex I (Gao et al., 1992), and thus, the difference between $J_{1',2'}$ and $J_{1',2''}$ or the sum of $J_{1',2'} + J_{1',2''}$ becomes smaller in duplex RI (Table 4). The DNA coupling constants $J_{3',4'}$ of duplex RI, especially those of purine residues, are larger than those in duplex I. This comparison is exemplified in Fig. 3, which contains COSY-35 spectra in the region of H4' (F2) and H3' (F1) for duplexes I and RI. Collectively, the coupling constant data support an intermediate C2'-endo and C3'-endo configuration for 2'-deoxyribose residues of the DNA strand in hybrid duplex RI. The dihedral angles δ of purine- or pyrimidine-associated sugars in duplex RI are in the range around 100°, while for duplex I, purine sugars have a more B-like sugar pucker (δ ~ 120°) and pyrimidine sugars have a less B-like sugar pucker (δ ~ 110°).

3D NOESY-NOESY spectrum

In the process of data analysis, it became clear that extensive overlaps in 2D proton spectra,

TABLE 4
$J_{1'2'}$, $J_{1'2''}$, AND $J_{3'4'}$ FOR DNA · RNA DUPLEX RI[a]

Residue	$J_{1'2'}$	$J_{1'2''}$	$J_{3'4'}$	Residue	$J_{1'2'}$
dC1	6.3	6.3	7.6	rG101	< 2
dG2	7.3	6.5	6.5	rC102	< 2
dC3	7.1	5.7	6.9	rG103	< 2
dG4	~ 7.3	~ 6.5	7.5	rC104	< 2
dT5	7.5	7.3	6.1	rA105	< 2
dT6	7.5	6.5	5.9	rA106	< 2
dT7	7.7	6.7	6.5	rA107	< 2
dT8	8.5	6.5	7.1	rA108	< 2
dG9	8.0	6.0	6.9	rC109	< 2
dC10	6.5	5.9	6.7	rG110	< 2
dG11	7.3	6.3	6.7	rC111	3.5
dC12	6.9	6.1	7.1	rG112	4.6

[a] Coupling constants were measured from a COSY-35 spectrum. Error estimation is ± 0.5 Hz. Some coupling constants of partially overlapped resonances were estimated. $J_{3'4'}$ couplings are apparent values.

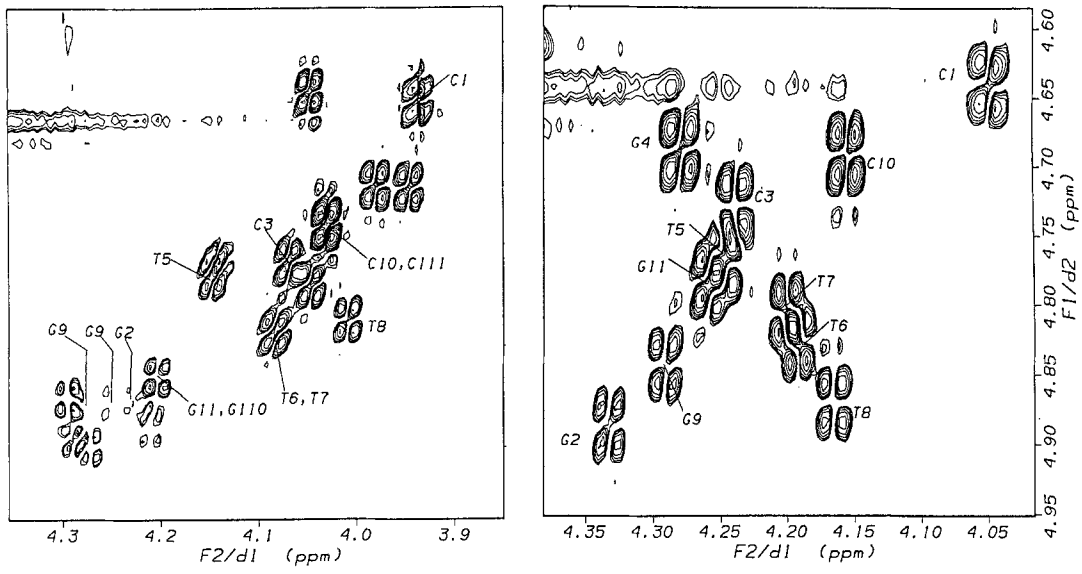

Fig. 3. H2',H2" decoupled COSY-35 spectra of DNA · DNA duplex I (left) and DNA · RNA duplex RI (right) in the region correlating H4' (F2) with H3' (F1). COSY cross peaks corresponding to the DNA strands d(CGCGTTTTGCGC) in duplexes I and RI are labeled. $J_{3'4'}$ values were estimated from these spectra with a digital resolution of 2.1 Hz.

especially in the region where ribonucleotide sugar protons resonate, rendered many NOE assignments ambiguous. This is shown in Fig. 4A, in which NOE cross peaks correlating G103, C104, G110 and C111 H8/H6 resonances with H2' and H3' protons were extensively superimposed. Homonuclear 3D NMR has been demonstrated to be useful in simplifying overcrowded 2D spectra for structure elucidation of proteins and deoxyoligonucleotides (Padilla et al., 1990; Gao and Burkhart, 1991; Radhakrishnan et al., 1991). These experiments are easy to implement and avoid the necessity for isotope labeling. For duplex RI, we elected to record a two-step incoherent magnetization transfer by using a NOESY-NOESY pulse sequence (Boelens et al., 1989) to avoid magnetization reduction due to small couplings between H1'/H2' protons in a ribose sugar. Our primary interest was to identify overlapped resonances and cross peaks and to evaluate the usefulness of the 3D NOESY-NOESY experiment as it applies to the elucidation of structural details of RNA.

Figure 4 illustrates the comparison of 2D NOESY and 3D NOESY-NOESY spectra of duplex RI for superimposed resonances of base protons of G103, C104, G110 and C111 at 7.49–7.53 ppm in F2 and H2' and H3' protons of C102, G103, C104 and G110 at 4.44–4.45 and 4.51–4.52 ppm in F1. The application of 3D NMR spectra for resolution enhancement requires that the frequencies of the spins in the third dimension that correlate to the overlapped 2D cross peaks be well separated. In practice, we prefer this frequency separation to be larger than 0.1 ppm if resolution is expected in a homonuclear proton 3D spectrum of 8 Hz resolution. For the aforementioned residues with overlapped H8,H6/H2' or H3' cross peaks, the H1' signals are well resolved (Fig. 4B). 3D NOESY-NOESY conveys connectivities from H1' (F3) to H2' or H3' (F2) of the same residue and then to other intra- and interresidue resonances (F1). Thus, by inspection of H1' planes at the frequencies of C111 (5.44 ppm), C104 (5.27 ppm) and G103 and G110

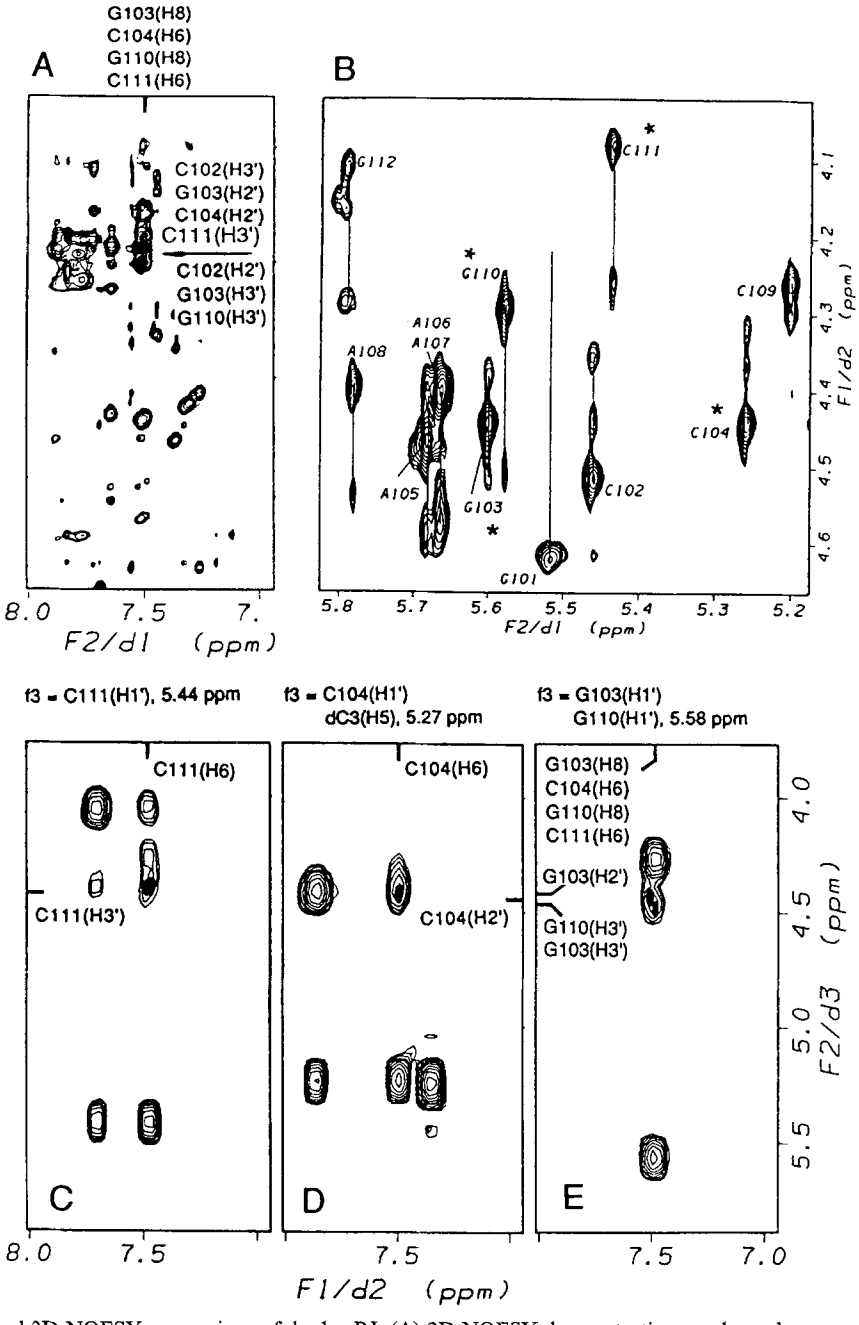

Fig. 4. 2D and 3D NOESY comparison of duplex RI. (A) 2D NOESY demonstrating overlapped proton resonances of G103, C104, G110 and C111. (B) 2D NOESY in the H1' region (F2) and the H2', H3', H4' region (F1) for the RNA strand in duplex RI. H1'/H2',H3' connectivities are indicated by solid lines. (C) 3D NOESY-NOESY plot at F1 = 5.44 ppm, where C111(H1') resonates. The 3D connectivity of C111(H1')/C111(H3')/C111(H6) is resolved in this plane. (D) 3D NOESY-NOESY plot at F1 = 5.27 ppm, where C104(H1') resonates. The 3D connectivity of C104(H1')/C104(H2')/ C104(H6) is resolved in this plane. (E) 3D NOESY-NOESY plot at F1 = 5.58 ppm, where G103(H1') and G111(H1') resonate. Partially overlapped 3D connectivities related to these two H1' protons are observed in this plane.

(5.58 ppm) in a 3D NOESY-NOESY spectrum, cross peaks corresponding to H6/H3' of C111 and H6/H2' of C104 can be unambiguously assigned, while those corresponding to H8/H3' of G103/G103, G103/C104, G110/G110 and G110/C111 can only be partially resolved in the 3D spectrum, due to closely located H1' resonances ($\Delta\delta$ 0.02 ppm) of G103 and G110 (Fig. 4C–E).

The overall improvement in the assignments of overlapped 2D cross peaks by 3D spectral analysis of duplex RI is summarized in Table 5. About 50% of the cross peaks cannot be resolved in the 2D spectra, more than 50% of which were separated in various regions of the 3D spectrum. For instance, of the 12 cross peaks of DNA base proton/H1' that were overlapped in the 2D spectra, 10 were assigned through the analyses of the H2' and H2" planes in the 3D NOESY-NOESY spectrum.

Analysis strategy for homonuclear 3D NOESY spectra

Three-dimensional connectivities in ribonucleotides are complex and it is important to develop strategies that will permit efficient assignment of 3D cross peaks. In our case, with the majority of the proton resonances identified and with knowledge of the global duplex helical structure, we sought to use 3D data to resolve ambiguous proton and cross-peak assignments. The analysis was initiated with a graphical representation of the proton–proton connectivities derived from an A-form RNA duplex. As shown in Fig. 5, pairs of protons that are predicted to be separated by less than 5 Å are connected by solid lines with the thickness of the line increasing as the distance decreases. The known residue numbers, proton names and resonance frequencies are labeled in the map (Fig. 5). Since a 3D cross peak is composed of any combination of three resonances, linked continuously in the connectivity map, the advantage of using such a diagram to guide the cross-peak identification is that the best solution in 3D data for resolving overlapped 2D cross peaks can be found easily. Employing this approach greatly facilitates searching various 3D spectral regions to locate the desired 3D cross peak. For example, to resolve the overlap between H8/H2' of G103 and H6/H2' of C104, the most effective spin-transfer pathways are through A105(H8)/C104(H2')/C104(H6) and C102(H1')/G103(H8)/G103(H2') (Fig. 5). Following such a diagram also permits the identification of the situation when 3D data fails to provide an answer. For instance, Fig. 5 indicates that there is no solution for overlapped cross peaks G110 H8/H1' and C111(H6)/G110(H1'), since all third spins linked to these two cross peaks are unresolved in

TABLE 5
SUMMARY OF 3D NOESY-NOESY ANALYSIS OF THE RNA STRAND IN DNA · RNA DUPLEX RI[a]

Spectral region	# of 2D cross peaks		# of peaks resolved
	Total	Overlaps	
base H(i)-base H5(i + 1)	3	2	2
adenine H2-sugar H1'	12	2	0
base H-sugar H1'(DNA)	23	12	10
base H-sugar H1'	23	8	5
base H-sugar H2'	23	13	8
base H-sugar H3'	23	10	7

[a] Analysis was based primarily on a 2D NOESY spectrum (100 ms mixing time). Results given are for the RNA strand in duplex RI, unless otherwise specified.

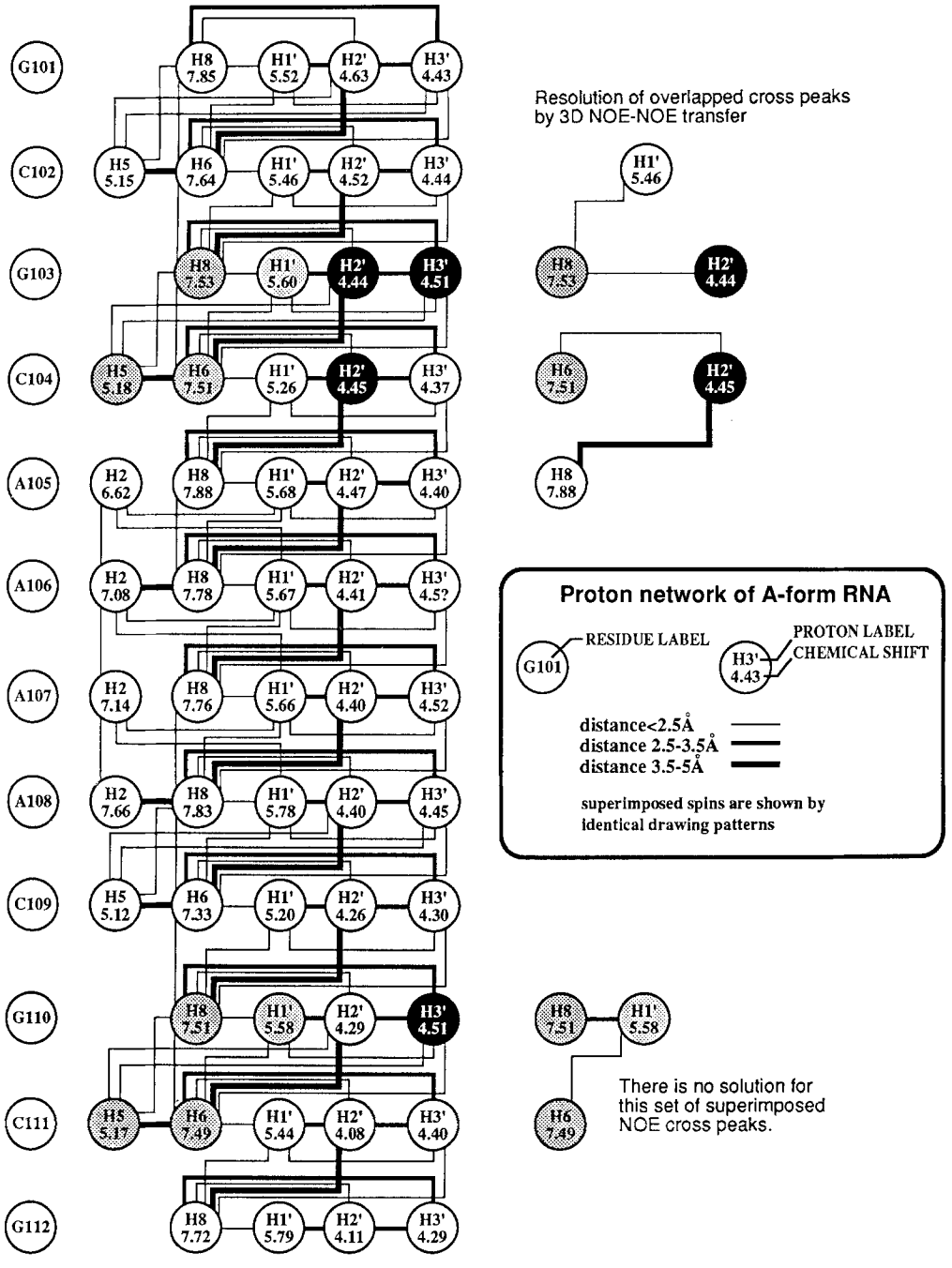

Fig. 5. Proton–proton connectivities of a right-handed A-form RNA duplex, used as a reference chart for efficient tracing of 3D connectivities.

the third dimension. In practice, when there are several pathways providing resolutions for superimposed 2D cross peaks, the most effective one (proton pairs connected by a thicker line)

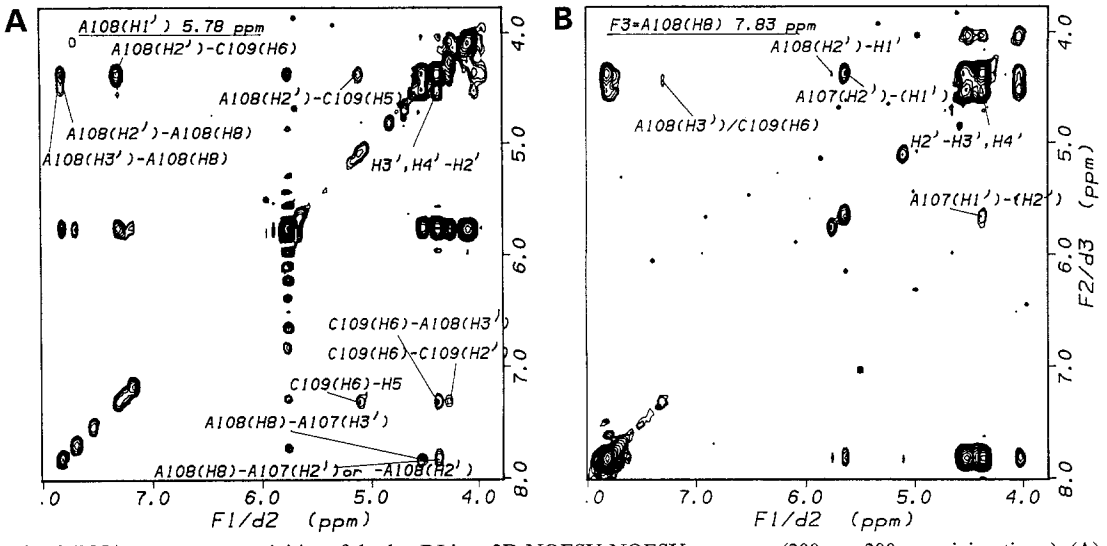

Fig. 6. RNA proton connectivities of duplex RI in a 3D NOESY-NOESY spectrum (200 ms-200 ms mixing times). (A) A 2D slice at F1 = 5.78 ppm, where A108(H1') resonates. True 3D cross peaks via A108(H1') are located off three lines: the diagonal line and lines passing through 5.78 ppm on either the F2 or F3 dimension; the assignments are given in the plot. (B) A 2D slice at F1 = 7.83 ppm, where A108(H8) resonates. Similarly as in A, true 3D cross peaks via A108(H8) are located off three lines: the diagonal line and lines passing through 7.83 ppm on either the F2 or F3 dimension; the assignments are given in the plot.

should be selected first. The second consideration is to minimize the effect of crosstalk in the 3D spectrum — the third spins linking to the two overlapped 2D cross peaks should have the largest possible separation in chemical shifts. The procedure described here also provides a basis for automation of 3D data analysis, using an assignment database obtainable from 2D spectra.

Previously, we reported a DNA proton assignment strategy by using homonuclear 3D NOESY-TOCSY or TOCSY-NOESY spectra (Radhakrishnan et al., 1991). The key to this strategy is the use of the H1' planes to follow the coupling connectivities from H1' to an intraresidue second spin and then to follow the spatial connectivities to the third spin. However, these 3D experiments would be insensitive for application to hybrid duplexes, due to the small couplings between the H1' and H2' of ribonucleotide residues. Thus, there are additional advantages that may be gained from 3D NOESY-NOESY spectra and these are illustrated by the application to the hybrid DNA · RNA duplex RI. Figure 6A shows a 2D plane at the A108(H1') frequency (5.28 ppm) and indicates true 3D connectivities through this resonance. We used the H2' and/or H2" planes to assign overlapped base proton/H1' cross peaks, as listed in Table 5. In contrast to 3D NOESY-COSY-type spectra, where cross peaks in base proton planes are usually absent due to the lack of coupling correlation from base protons, the base proton planes of the 3D NOESY-NOESY spectrum contain many connectivities that provide additional spectral resolution for overlapped cross peaks. A base proton 2D plane at 7.83 ppm (H8 of A108) is illustrated in Fig. 6B. In this plane, connectivities linking A108(H8)/A108(H2')/A108(H1'), A108(H8)/A107(H2')/A107(H1'), A108(H8)/A108(H3')/C109(H6) and A108(H8)/A108(H2')/A108(H3', H4') were identified at positions F1 ≠ F2 ≠ F3 (Fig. 6B). An observation that bears comment is that weak NOEs observed in 2D spectra are often missing from the 3D spectrum. Moreover, 3D spectral resolution

used in this study does not warrant definitive assignments of NOEs related to H3', H4' and H5',H5" protons. This problem may be alleviated by the use of a much reduced spectral width (5 ppm) for RNA sequences, which lack upfield resonances of sugar H2',H2" protons.

CONCLUSIONS

We have presented a study of a hybrid DNA · RNA duplex RI from two aspects. First, a combination of 2D and 3D NMR experiments was applied to derive a set of NMR parameters that permit detailed structural and conformational analyses of the RI duplex. The hybrid duplex RI, when compared to the DNA · DNA duplex I, showed significant spectral deviations that reflect a major structural readjustment when a DNA strand binds to an RNA strand, as opposed to binding of a DNA strand to a DNA strand. The two strands of duplex RI exhibited distinctly different NMR parameters, with the DNA strand possessing more B-form character and the RNA strand possessing more A-form character. However, some NMR data cannot be reconciled by either canonical A- or B-form duplexes. The question raised from these results is how the heterogeneous conformation is being accommodated in the sequence to give a unique overall structure of the hybrid duplex. While our conclusions are in general agreement with those reported by Chou et al. (1989), the application of higher dimensional NMR and improved spectroscopic methods permits the derivation of a more detailed and complete set of experimental parameters.

Following the submission of this manuscript, an NMR study of an octamer DNA · RNA hybrid duplex suggested that the RNA strand retains an N-type structure with the sugars adopting a C3'-endo (A-form) conformation. Furthermore, the DNA strand was found to assume neither an all-C2'-endo B-type nor a C3'-endo A-type conformation (Salazar et al., 1993). These results are in keeping with the findings in the studies reported herein.

Acquisition of these parameters is crucial for developing an accurate 3D structural model of the hybrid duplex. Thus, the 3D NOESY-NOESY experiment of the RNA molecule (the RNA strand in duplex RI) was undertaken and analyzed to resolve many ambiguous assignments from the 2D data, including over 50% of the overlapped 2D cross peaks of sequential NOEs. The application of a useful strategy that combines the use of 2D NMR data and the known structural information for efficient 3D spectral analyses is demonstrated. These results provide a basis for the evaluation of local conformations and high-resolution structure determination.

ACKNOWLEDGEMENTS

We thank Dr. David Hoffman (Duke University) for the initial enzymatic synthesis of the RNA strand in duplex RI, Mr. Adrian Pipe (Glaxo Group Research, U.K.) for providing the material by chemical synthesis, and Dr. Jeff Rice (University of Houston) for careful reading of the manuscript.

REFERENCES

Arnott, S., Chandrasekharan, R., Millane, R.P. and Park, H.-S. (1986) *J. Mol. Biol.*, **188**, 631–640.
Arnott, S. and Hukins, D.W. (1972) *Biochem. Biophys. Res. Commun.*, **47**, 1504–1509.
Arnott, S. and Hukins, D.W. (1973) *J. Mol. Biol.*, **81**, 93–105.
Benevides, J.M. and Thomas Jr., G.J. (1988) *Biochemistry*, **27**, 3868–3873.

Boelens, R., Vuister, G.W., Koning, T.M.G. and Kaptein, R. (1989) *J. Am. Chem. Soc.*, **111**, 8525–8526.
Chen, S.-M., Leupin, W. and Chazin, W.J. (1992) *Int. J. Biol. Macromol.*, **14**, 57–63.
Chou, S.-H., Flynn, P. and Reid, B. (1989) *Biochemistry*, **28**, 2435–2443.
Egli, M., Usman, N., Zang, S. and Rich, A. (1992) *Proc. Natl. Acad. Sci. USA*, **89**, 534–538.
Gao, X. and Burkhart, W. (1991) *Biochemistry*, **30**, 7730–7739.
Gao, X., Brown, F.K., Jeffs, P.W., Bischofberger, N., Lin, K.-Y., Pipe, A.J. and Noble, S.A. (1992) *Biochemistry*, **31**, 6228–6236.
Gray, D.M. and Ratcliff, R.L. (1975) *Biopolymers*, **14**, 487–498.
Gupta, G., Sarma, M.H. and Sarma, R.H. (1985) *J. Mol. Biol.*, **186**, 463–469.
Hall, K.B. and McLaughlin, L.W. (1991) *Biochemistry*, **30**, 10606–10613.
Happ, C.S., Happ, E., Clore, G.M. and Gronenborn, A.M. (1988) *FEBS Lett.*, **236**, 62–70.
Heus, H.A. and Pardi, A. (1991) *J. Am. Chem. Soc.*, **113**, 4360–4361.
Hoffman, D.W., Colvin, R.A., Garcia-Blanco, M.A. and White, S.W. (1993) *Biochemistry*, **32**, 1096–1104.
Jaishree, T.N., Van der Marel, G.A., Van Boom, J.H. and Wang, A.H.-J. (1993) *Biochemistry*, **32**, 4903–4911.
Katahira, M., Lee, S.J., Kobayashi, Y. and Thomas Jr., G.J. (1990) *J. Am. Chem. Soc.*, **112**, 4508–4512.
Katahira, M., Sugeta, H. and Kyogoku, Y. (1990) *Nucleic Acids Res.*, **18**, 613–618.
Mellema, J.-R., Haasnoot, C.A.G., Van der Marel, G.A., Wille, G., Van Boeckel, C.A.A., Van Boom, J.H. and Altona, C. (1983) *Nucleic Acids Res.*, **11**, 5717–5738.
Milman, G., Langridge, R. and Chamberlin, M.J. (1967) *Proc. Natl. Acad. Sci. USA*, **57**, 1804–1810.
Nakamura, H., Oda, Y., Iwai, S., Inoue, H., Ohtsuka, E., Kanaya, S., Kimura, S., Katsuda, C., Katayagi, K., Morikawa, K., Miyashiro, H. and Ikehara, M. (1991) *Proc. Natl. Acad. Sci. USA*, **88**, 11535–11539.
Neuhaus, D. and Williamson, M. (1989) *The Overhauser Effect in Structural and Conformational Analysis*, VCH Publishers, New York, NY, pp. 104–110.
O'Brien, E.J. and MacEwen, A. (1970) *J. Mol. Biol.*, **48**, 243–261.
Padilla, A., Vuister, G.W., Boelens, R., Kleywegt, G.J., Cave, A., Parello, J. and Kaptein, R. (1990) *J. Am. Chem. Soc.*, **112**, 5024–5030.
Radhakrishnan, I., Patel, D.J. and Gao, X. (1991) *J. Am. Chem. Soc.*, **113**, 8542–8544.
Reid, D.G., Salisbury, S.A., Brown, T., Williams, D.H., Vasseur, J.-J., Rayner, B. and Imbach, J.-L. (1983) *Eur. J. Biochem.*, **135**, 307–314.
Salazar, M., Fedoroff, O.Y., Miller, J.M., Ribeiro, N.S. and Reid, B.R. (1993) *Biochemistry*, **32**, 4207–4215.
Shindo, H. and Matsumoto, U. (1984) *J. Biol. Chem.*, **259**, 8682–8684.
Sklenář, V., Miyashiro, H., Zon, G., Miles, H.T. and Bax, A. (1986) *FEBS Lett.*, **208**, 94–98.
Steely, H.T., Gray, D.M. and Ratcliff, R.L. (1986) *Nucleic Acids Res.*, **14**, 10071–10090.
Wang, A.H.-J., Fujii, S., Van Boom, J.H., Van der Marel, G.A., Van Boeckel, C.A.A. and Rich, A. (1982) *Nature*, **299**, 601–604.
Wang, A.C., Kim, S.G., Flynn, P.F., Chou, S.H., Orban, J. and Reid, B.R. (1992) *Biochemistry*, **31**, 3940–3946.
Wüthrich, K. (1986) *NMR of Proteins and Nucleic Acids*, Wiley, New York, NY.
Zimmerman, S.B. and Pheiffer, B.H. (1981) *Proc. Natl. Acad. Sci. USA*, **78**, 78–82.